

Effects of the Wire Feeding Speed on the Mechanical Properties and Electrochemical Corrosion Behaviors of a Hybrid Laser-MAG Welded X90 Pipeline Steel

Mei Yang^{1,*}, Jingxiang Lu¹, Yang Li², Jian Tan³, Wenhao Zhang¹, Honglang Yang¹

¹ School of New Energy and Materials, Southwest Petroleum University, Cheng'du 610500, China

² Sichuan petroleum Engineering Construction Co. Ltd, Cheng'du 610000, China

³ Engineering Technology Research Institute, Petro China Southwest Oil and Gas Field Company, Deyang618300, China

*E-mail: 380056676@qq.com

Received: 18 June 2020 / Accepted: 9 August 2020 / Published: 31 August 2020

This paper studies the welding of X90 pipeline steel with ER100S-G welding wire via laser-metal active gas arc (laser-MAG) hybrid welding and explores the effects of three wire feeding speeds (8.5 mm/s, 9 mm/s, and 9.5 mm/s) on the microstructure, mechanical properties and corrosion resistance of the weld joints. The results demonstrate that the microstructure of the weld is composed mainly of acicular ferrite (AF) and massive ferrite (MF). The structure of the heat-affected zone (HAZ) is composed mainly of granular bainite (GB) and acicular ferrite (AF). As the wire feeding speed is increased, the weld and HAZ grains grow significantly, while the ultimate tensile strength and microhardness decrease. Polarization curves were obtained and electrochemical impedance spectroscopy (EIS) was conducted on welds and base metals. The base material has the highest corrosion resistance, and the corrosion resistance of the welds decreased as the grains grew.

Keywords: Hybrid laser-MAG welding; Mechanical properties; X90; Electrochemical experiments;

1. INTRODUCTION

With the rapid evolution of the oil and gas industry in recent years, the construction of pipelines has trended toward large diameters, long distances, low temperatures, and thickening of submarine pipelines. To reduce the pipeline engineering and transportation costs and increase transport safety, improvement of the grade of pipeline steel to realize high-pressure, large-caliber and long-distance pipeline transportation has become an inevitable trend in pipeline construction. With the rapid advancement of the oil and gas industry, high-grade pipeline steel has been continuously developed. [1-3] As a high-grade petroleum pipeline steel, X90 is utilized with added trace alloy elements (such as Ni,

Mo, and Cr) and a suitable thermomechanical controlled processing (TMCP) process to obtain fine and uniform crystal grains, which are mainly low-carbon bainite. X90 steel has broad application prospects due to its high strength and toughness and satisfactory weldability. [4,5]

Studies have been conducted on the arc welding of X90-grade pipeline steel, but conventional arc welding has a shallower penetration depth, is prone to impervious welding, requires large heat input and produces large deformations. To improve the weld microstructure and performance, the current development trends are mainly the addition alloy elements in welds, the development the filler materials, and the use of new welding processes. [6-8] Laser-arc hybrid welding is a newly developed welding technology that combines heat sources of arc and laser to realize high power density, small heat input, fast welding speed, and weld seams. Laser-arc hybrid welding has substantial advantages in the welding production of medium and thick pipes, which include large penetration depth and satisfactory gap adaptability. [9,10] Seffer et al. [11] combined laser and gas-shielded metal arc welding to realize X70 sheet welding. The thermal cycle and cooling rate of welding affect in the change of the microstructure. Studies on X90 welding focus mainly on the weld structure and performance. [12,13] Zhao et al. [14] and others showed that the coarse-grained heat-affected zone microstructure of welding thermal cycle simulation specimens consists mainly of granular bainite and lath bainite. Guo et al. [15] showed that the coarse-grained heat-affected zone microstructure changed after the thermal cycle of X90 steel welding. As the heat input decreased, the microstructure, which was dominated by lath bainite, was significantly refined, and the impact toughness significantly increased.

Weld joint failure and corrosion have always been important issues in the pipeline transportation industry due to their reduction of the pipeline lifetime. Few studies have been conducted on laser-metal active gas arc (laser-MAG) hybrid welding joints of X90-grade pipeline steel and corrosion resistance after welding. This paper conducts laser-MAG welding on X90 pipeline steel and investigates the mechanical properties, microstructure and corrosion resistance of X90 pipeline steel laser-MAG hybrid welding joints at various wire feeding speeds.

2. MATERIALS AND METHODS

2.1 Materials

For the experiment, an X90 steel plate with a thickness of 16.6 mm was used. The chemical composition is presented in Table 1. According to the principle of equal-strength matching, a butt weld test was conducted with a welding wire of model ER100S-G and a diameter of 1.6 mm. Table 1 presents the ER100S-G chemical composition; the yield strength is 670 MPa, and the tensile strength is 830 MPa.

Table 1. Chemical composition of X90 pipeline steel and ER100S-G welding wire (Wt%)

Element	C	Mn	Si	P	S	Cr	Ni	Mo	Ti	V	Al	Cu	Fe
X90	0.05	1.9	0.25	0.008	0.002	Cr+Ni+Mo+Ti<1				/	/	/	Bal.
ER100S-G	0.08	1.6	0.50	0.005	0.009	0.3	1.5	0.25	0.005	0.09	0.004	0.15	Bal.

2.2 Welding process

This experiment uses a combination of laser in front and perpendicular to the weldment and arc in the back. During the experiment, the fiber laser-MAG side-axis composite system is used for butt welding. A schematic diagram of the welding process is shown in Fig. 1(b). The MAG welding torch is at an angle of 30° with the laser beam, and the laser beam is maintained perpendicular to the surface of the weldment during the welding process, with the laser in front and the arc behind. The MAG arc welding uses DC reverse connection, and the welding speed is 11 mm/s. The welding groove is shown in Fig. 1(a); the pitch is 1.2 mm, and the angle of the groove is 45° . The shielding gas that was used in the experiment was comprised of 18% CO_2 and 82% Ar, and the flow rate was 40 L/min. The welding parameters are listed in Table 2.

Table 2. Laser-MAG welding process parameters

No.	Wire feeding rate(mm/s)	Defocusing distance (mm)	Laser power (KW)	Laser-wire distance (mm)	Welding current (A)	Welding voltage (V)	
Backing weld	1	6.7	0	3.0	3	147	18
	2	6.7	0	3.0	3	147	18
	3	6.7	0	3.0	3	147	18
Filling and cosmetic weld	1	8.5	0	1.0	3	155	18.5
	2	9.0	0	1.0	3	163	18.4
	3	9.5	0	1.0	3	169	19

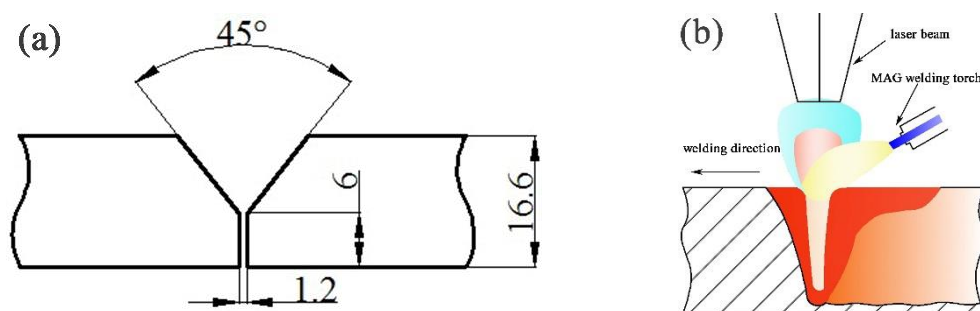


Figure 1. Welding groove (a) and a schematic diagram of the welding process (b)

2.3 Test

The sample was cut with a wire cutter, ground with water sandpaper of various specifications, and polished with a diamond polishing paste with a particle size of $1.5\mu\text{m}$. Etching was conducted using an etchant with a distribution ratio of $\text{HNO}_3 : \text{C}_2\text{H}_5\text{OH} = 4 : 96$. Then, the sample was washed with alcohol and blown dry. Optical microscopy(OM) (DME-300M), scanning electron microscopy(SEM) (ZEISS EV0 MA15), and X-ray diffraction(XRD) (X'pert PRO) were used to observe the microstructure and

phase analysis of the weld. A digital microhardness tester was utilized to measure the Vickers microhardness (HVS-1000) from the weld to the base metal after 10 s under a 500 g load. The mechanical properties of the weld butt joints were evaluated by conducting standard transverse tensile tests using a universal testing machine (SHT4605) with a strain rate of 2 mm/min. A schematic diagram of the tensile specimens is shown in Fig. 2.

The base metal and the weld zones under the three welding processes were processed into 5 mm×5 mm×5 mm test samples, and a 3.5% NaCl solution was used as the corrosion system. An electrochemical corrosion test was conducted using an electrochemical integrated test system (PGSTAT 302N). The potentiodynamic polarization test side scan range is -0.3 V ~ 0.33 V, and the scanning rate is 0.33 mV/s. Polarization curve and electrochemical impedance spectroscopy(EIS) measurements were conducted. The corrosion resistances of the welded joints under three wire feeding speeds were investigated.

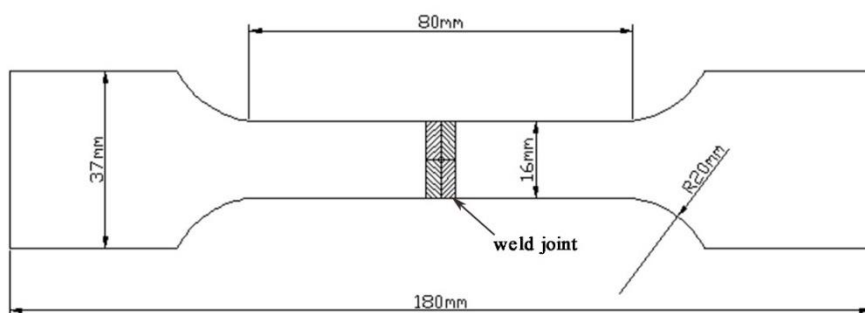


Figure 2. Schematic diagram of the tensile specimens

3. RESULTS AND DISCUSSION

3.1 Microstructure of the weld seam and the HAZ

Aiming at the joint, the effects of the wire feeding speed on the microstructure of the welded joint and the heat-affected zone (HAZ) were investigated mainly by observing the morphology of the microstructures in the region of the weld and in the HAZ.

Fig. 3 shows the microstructures of the weld under three wire feeding speeds. According to Fig. 3(a ~ f), the microstructures of the central region of the weld under three wire feeding speeds are acicular ferrite (AF), massive ferrite (MF), and an M/A island structure in the massive ferrite grains. During the formation of bainite, carbon is gradually concentrated in the retained austenite. Carbon enrichment results in increased austenite stability. [16] After cooling, a spot of island-shaped austenite distributed in the massive ferrite grains. This island-like M/A component consisted of martensite and retained austenite. To determine the phase composition of the weld, an XRD test was conducted on the weld. Fig. 4 presents the results of the XRD analysis of the weld metal. After comparison with a standard PDF card, the phase structure is α -Fe. Comparing the metallographic structure and SEM results of the weld at three wire feeding speeds, with the wire feeding speed increase, the AF content decreases. The welding

current and the welding heat input increase, and the weld joint cooling rate decreases. Therefore, the stability of austenite decreases, and a high-temperature transformation occurs. Since the weld structure remains at a high temperature for a long time, more high-temperature transformation structures, such as proeutectoid ferrite, are generated, which reduces the amount of AF.[17,18] As the wire feeding speed increases, the grains of the weld grow due to longer periods at high temperatures. Therefore, under the condition that the weld was formed well, reducing the wire feeding speed is beneficial for obtaining a fine weld structure.

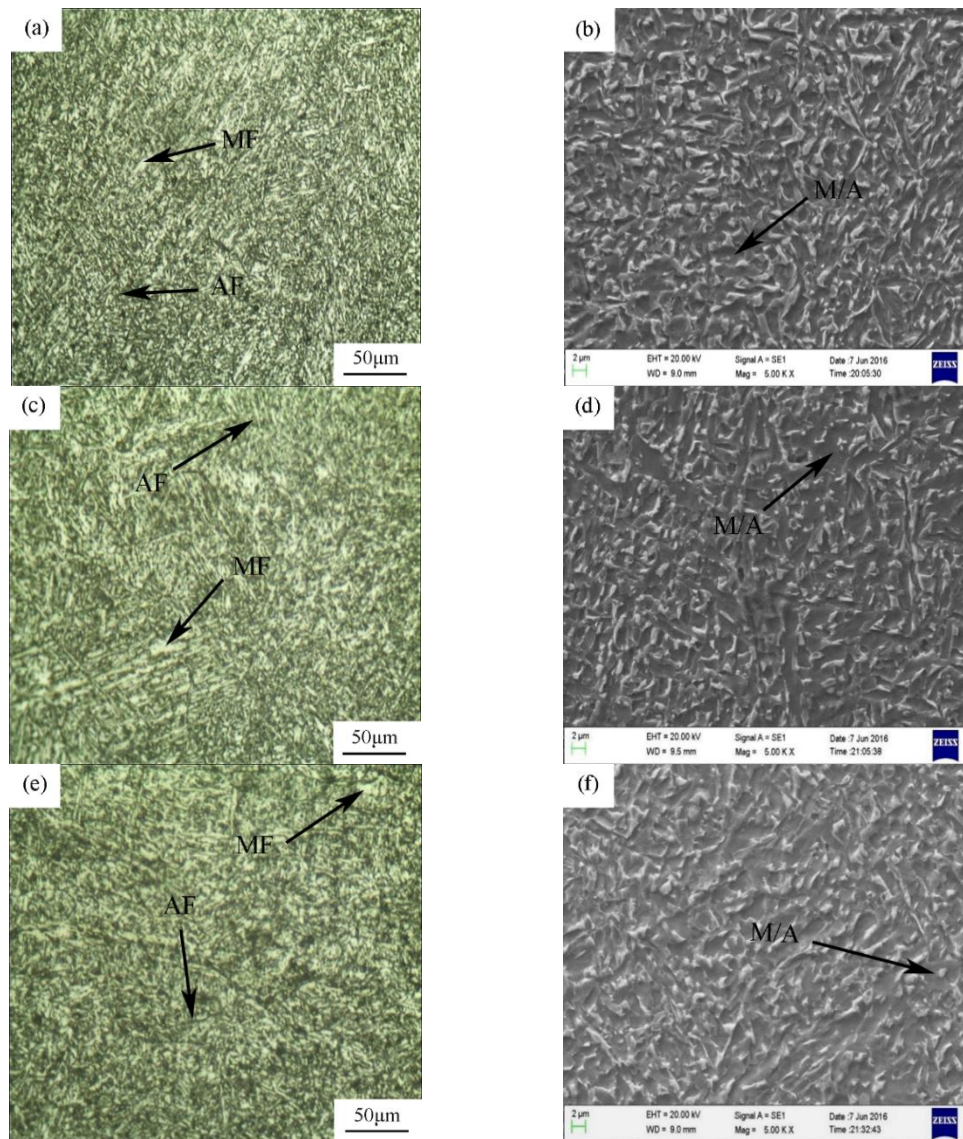


Figure 3. OM and SEM microstructure of the weld zone with three wire feed speeds (a)(b)8.5mm/s; (c)(d)9mm/s; (e)(f) 9.5mm/s

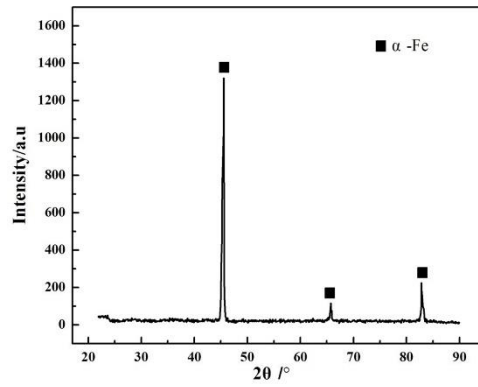
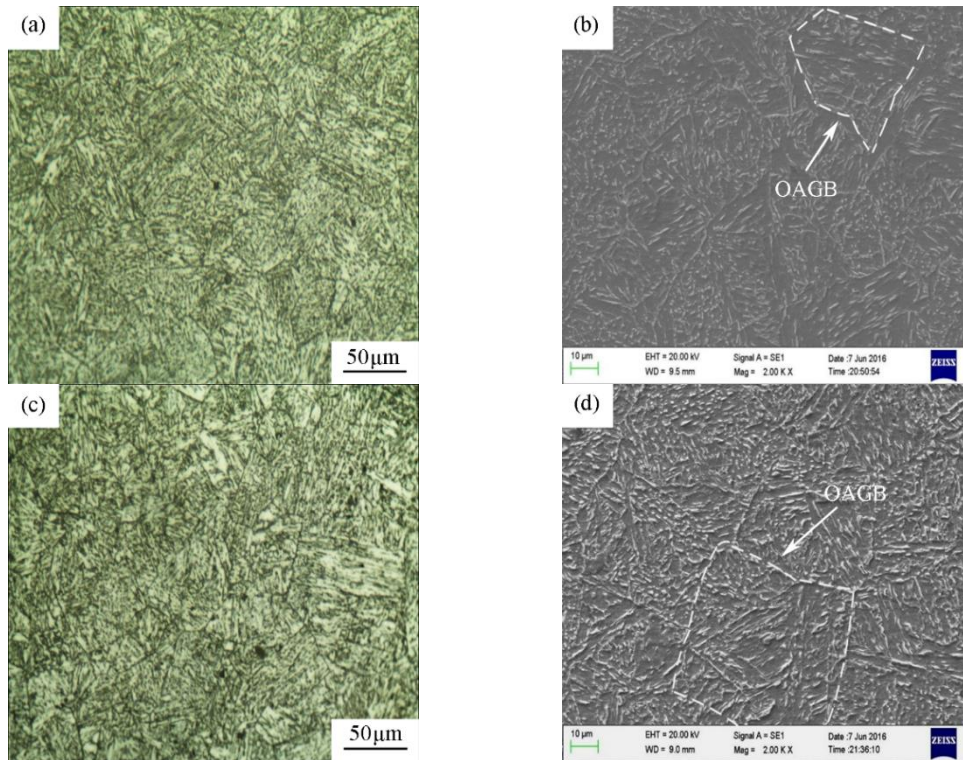


Figure 4. XRD test results of weld

Fig. 5(a ~ f) presents the OM and SEM results of HAZ. The HAZ microstructure is consisted granular bainite (GB), acicular ferrite (AF), a scattered blocky M/A constituent and a small amount of pearlite. As wire feeding speeds increase from 8.5 mm/s to 9 mm/s and 9.5 mm/s, the grains in HAZ grow. The original austenite grain boundaries (OAGB) easily evolve from the original flat and smooth shape to a regular polygon. The amount of lath bainite increases, and the lath bainite becomes thicker and larger. This is because the wire feeding speed determines the welding current. The welding heat input increases with the increase of the welding current; hence, the HAZ remains longer in the high-temperature zone.



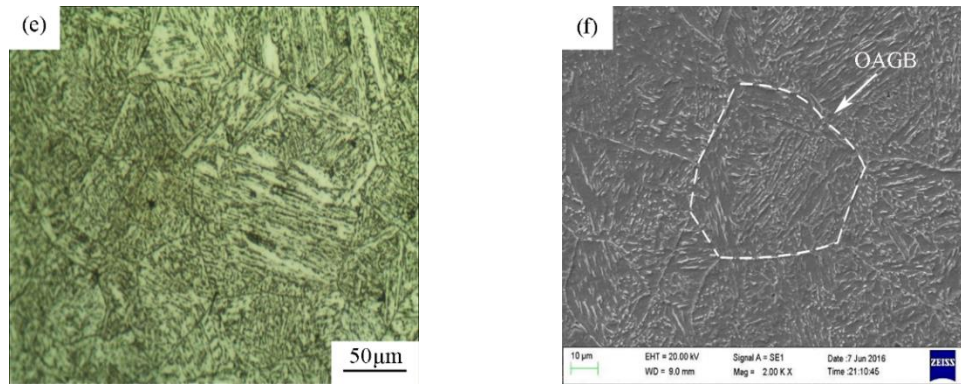


Figure 5. OM and SEM results of the HAZ with three wire feed speeds (a)(b)8.5mm/s; (c)(d)9mm/s; (e)(f) 9.5mm/s

3.2 Mechanical properties

3.2.1 Hardness of weld seam

Fig. 6 presents the microhardness results for the weld joint. The hardness decreases initially and subsequently increases from the weld to the base metal. During the welding process, areas of the welded joint undergo different thermal cycles; hence, the areas differ in terms of microstructure and grain size. Therefore, the microhardness also differs among regions. The average hardness of the weld joint is presented in Table 3. As the wire feeding speed was increased from 8.5 mm/s to 9.0 mm/s and 9.5 mm/s, the average microhardness of the weld zone decreased from 280.93 HV to 277.77 HV and 275.84 HV, respectively, and the average microhardness of the HAZ decreased from 258 HV to 253.95 HV and 249.28 HV, respectively. Combined with the microstructure, the increase of the wire feeding speed led to the increase of the heat input. The increased cooling time and heat input causes the grain size to increase. The microhardnesses of the HAZ and the weld decreased as the wire feeding speeds increased.

Table 3. Average microhardness of welded joints with three wire feed speeds

Wire feeding speed(mm/s)	FZ(HV _{0.1})	HAZ(HV _{0.1})	BM(HV _{0.1})
8.5	280.93	258	273.79
9	277.77	253.95	273.27
9.5	275.84	249.28	273.29

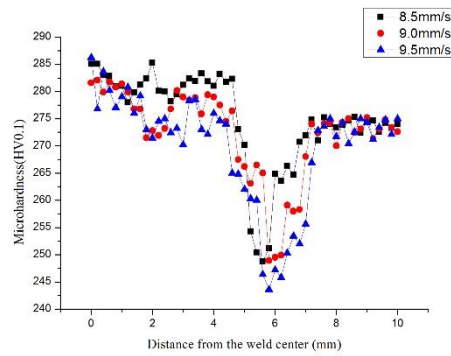


Figure 6. Welded joint hardness test results with three wire feeding speeds

3.2.2 Tensile properties of weld joints

Table 4 and Fig. 7 present the tensile test results of the weld joint and base metal at three wire feeding speeds. The fracture locations of the welded joints at the three wire feeding speeds are heat-affected zones. According to Table 4, the average tensile strength and the average yield strength of the welded joints at 8.5 mm/s are the highest among the three groups, which are equivalent to those of the base metal, namely, 816.6 MPa and 741.6 MPa. The average tensile strength of the welded joint at 9 mm/s is 763.2 MPa, which was 92.9% that of the base material, and the average yield strength was 694.2 MPa. The average tensile strength of the welded joint at 9.5 mm/s is 800 MPa, which is 97.3% that of the base metal, and the average yield strength is 736.6 MPa. Combined with the microstructure of HAZ, with the wire feeding speed increase, the heat input increases, thereby resulting in coarser HAZ grains, and the amount of lath bainite increases. Cracks usually initiate and extend along the alignment direction of the lath bainite. Therefore, the tensile strength tends to decrease as the wire feeding speed increases.

Table 4. Tensile test results of the base metal and weld samples

	No.	Tensile strength R_m /MPa		Yield strength R_f /MPa		Fracture location
			Average		Average	
Base metal	0-1	825		750		—
	0-2	830	821.6	750	746.6	—
	0-3	810		740		—
8.5mm/s	1-1	825		745		HAZ
	1-2	815	816.6	740	741.6	HAZ
	1-3	810		740		HAZ
9.0mm/s	2-1	795		735		HAZ
	2-2	795	800.0	735	736.6	HAZ
	2-3	810		740		HAZ
9.5mm/s	3-1	760		690		HAZ
	3-2	755	763.3	690	693.3	HAZ
	3-3	775		700		HAZ

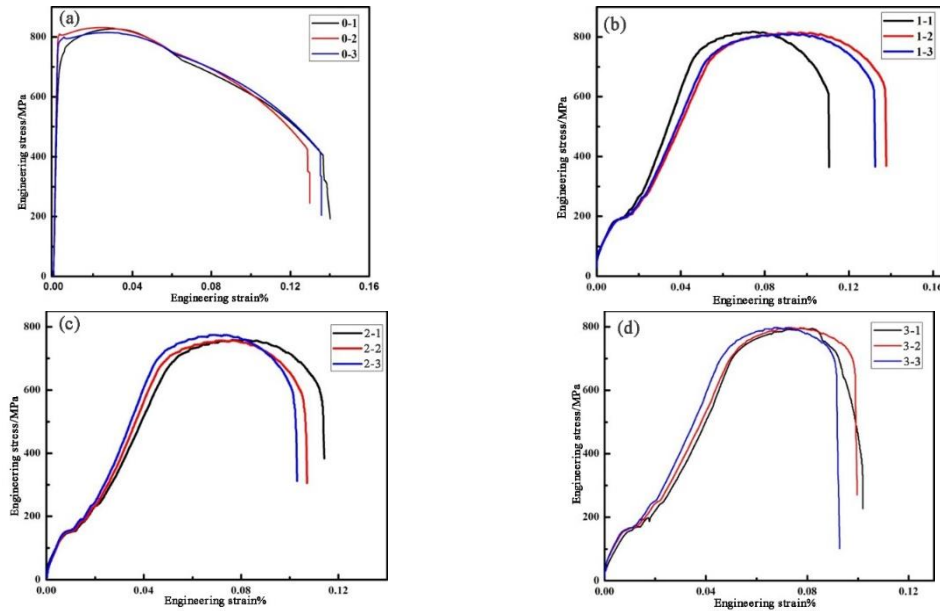


Figure 7. Tensile test results of the base metal and weld samples (a) base material; (b) 8.5 mm/s; (c) 9 mm/s; and (d) 9.5 mm/s

3.3 Corrosion resistance test

3.3.1 Polarization curve test

Weld joints are susceptible to corrosion for several reasons, which include mainly the chemical composition of the weld, changes in the metallurgical structure, and the residual stress levels in the welded structure. To predict the full service life of a welded structure in a corrosive environment, the corrosion rate or corrosion sensitivity of the welded structure must be determined prior to use. ^[19] Fig. 8 presents a polarization curve that was obtained by conducting a polarization test on a base metal and a weld joint metal at three wire feeding speeds in a 3.5% NaCl solution.

According to Fig. 8, the polarization curves of the three groups of weld samples and the base metal in the 3.5% NaCl solution are similar, and no passivation behavior occurs because X90 is a low-alloy steel and does not exhibit passivation behavior in a 3wt% NaCl solution at room temperature; [20,21] hence, they have the characteristics of an activated state. The electrochemical corrosion test parameters of the weld metal samples and the base metal were fit. The results are presented in Table 5. According to Table 5, the base metal has the highest corrosion potential of -0.515 V. As the wire feeding speed increased from 8.5 mm/s to 9.0 mm/s to 9.5 mm/s, the weld corrosion potential decreased from -0.652 V to -0.698 V to -0.717 V, respectively. According to Table 5, the corrosion current density of the base metal is 1.34×10^{-3} mA/cm². The weld corrosion current density gradually increased as the wire feeding speed increased. The corrosion current density of the weld at 8.5 mm/s is 4.67×10^{-3} mA/cm², the corrosion current density of the weld at 8.5 mm/s is 5.62×10^{-3} mA/cm², and the corrosion current density of the weld at 9.5 mm/s is 8.91×10^{-3} mA/cm². The corrosion current density of the base metal is significantly lower than the corrosion current densities of the weld areas of the three groups of joints; hence, the corrosion resistance of the base metal is higher than those of the weld areas of the three groups

of joints, and the degree of corrosion is the lowest. As the wire feeding speed increased, the corrosion current density of the weld zone gradually increased, and the corrosion resistance decreased. Studies have suggested that [22-24] due to the large differences in the state of the weld structure and the base metal, the electrochemical performances differ substantially between the two regions, and the result will cause local selective corrosion of the joint. According to other studies, the acicular ferrite matrix metal shows a large current density. [25.26] Compared with the base metal structure, it is an anode, which corroded before the base metal. Therefore, the corrosion resistance of the base metal is higher than those of the weld. The welding current and the welding heat input increase with the wire feeding speed. The large heat input causes the element distribution in the structure to become nonuniform, and the degree of element segregation increases, which will reduce the weld corrosion resistance. Studies have shown that via grain refinement, the rate of the anode reaction can be controlled, but it has minimal effect the rate of the cathode reaction. [27] With the increases of wire feeding speed, the coarsening of the grains causes the anode reaction to accelerate, which reduces the corrosion resistance.

Table 5. Corrosion potential E_{corr} and corrosion current density I_{corr} of the base metal and weld metal at three wire feeding speeds.

Parameter	Base metal	8.5mm/s	9.0mm/s	9.5mm/s
$E_{\text{corr}}/(\text{V})$	-0.515	-0.652	-0.698	-0.717
$I_{\text{corr}}/(\text{mA}/\text{cm}^2)$	1.34×10^{-3}	4.67×10^{-3}	5.62×10^{-3}	8.91×10^{-3}

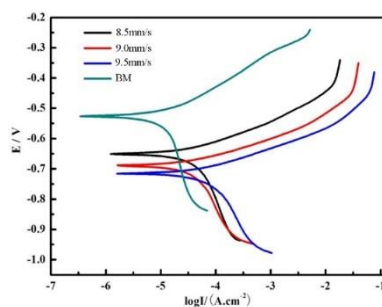


Figure 8. Polarization curves of the base metal and weld metal samples

3.3.2 Electrochemical impedance spectroscopy

Fig. 9 presents the EIS test results of the weld metal samples with three wire feeding speeds and of the base metal in 3.5% NaCl solution. According to Fig. 9, the four impedance spectra of the weld metal samples at three wire feeding speeds and of the base metal all show a single-capacitance reactance arc, which corresponds to a single time-constant response mode. The test results demonstrate that there is only one reaction mode. From large to small curve radius, the samples are ordered as follows: base metal > 8.5 mm/s > 9 mm/s > 9.5 mm/s. The presence of a peak in a wider frequency range corresponds to a higher corrosion resistance of the sample; [28] hence, the surface of the base metal has higher corrosion resistance than the three sets of joint welding areas.

Table 6. Charge transfer resistance

No.	$R_{ct}/(\Omega.cm^2)$	Ratio(%)
Base metal	2030	100
8.5 mm/s	1461	71.97
9.0 mm/s	1051	51.77
9.5 mm/s	813	40.05

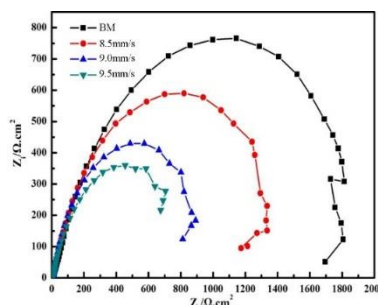


Figure 9. Electrochemical impedance spectroscopy diagrams of the base metal and weld samples

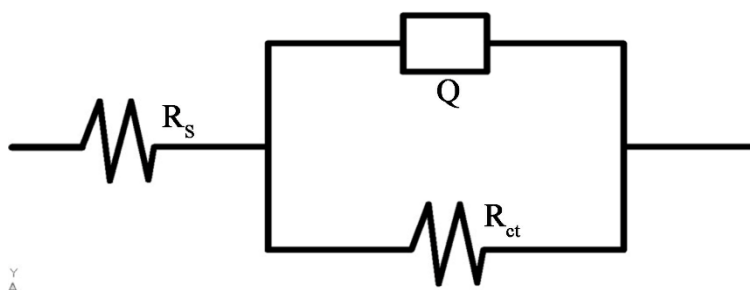


Figure 10. Equivalent electric circuit.

Fig. 10 presents the equivalent electric circuit diagram of this test, where R_{ct} represents the interface charge transfer resistance. The larger the value of R_{ct} , the higher the resistance that is encountered by the interface corrosion reaction and, thus, the higher the corrosion resistance of the joint at this stage. The R_{ct} values that were obtained by fitting the curve using the equivalent circuit diagram are presented in Table 6. According to Table 6, the base metal has the highest R_{ct} value of $2030\Omega.cm^2$. As the wire feeding speed increased from 8.5 mm/s to 9.0 mm/s to 9.5 mm/s, the weld R_{ct} value decreased from $1461\Omega.cm^2$ to $1051\Omega.cm^2$ to $813\Omega.cm^2$. The resistance usually increases as the grain boundary density increases. As the wire feeding speed increases, the welding heat input increases, grain coarsening results in a lower grain boundary density, the R_{ct} value decreases and the corrosion resistance decreases. This is consistent with the results from the polarization experiments. Hence, the wire feeding speed increase will lead to the corrosion resistance decrease of the weld.

4. CONCLUSIONS

In this study, X90 pipeline steel was welded via laser-MAG hybrid welding to explore the effects of the wire feeding speed on the microstructure, mechanical properties and corrosion resistance of the weld joints.

The weld microstructure is acicular ferrite; a massive ferrite and M/A island structure is observed in the massive ferrite grains. The structure of the HAZ consists of GB, AF, a scattered blocky M/A constituent and a small quantity of pearlite. As the wire feeding speed is increased from 8.5 mm/s to 9 mm/s and 9.5 mm/s, the welding current increase and the heat input increase, and the grains of the weld and HAZ exhibit growth trends due to longer periods at high temperatures.

Increasing the wire feeding speed from 8.5 mm/s to 9 mm/s and 9.5 mm/s cause an increases in the heat input and decreases in the microhardness and ultimate tensile strength of the weld and the HAZ due to grain growth. The ultimate tensile strength of the weld reaches 816.6 MPa when the wire feeding speed is 8.5 mm/s.

The polarization curve and impedance experiment results demonstrate that the base material has the highest corrosion resistance, the lowest self-corrosion current density and the largest R_{ct} value. With the increase of the wire feeding speed from 8.5 mm/s to 9 mm/s and 9.5 mm/s, the heat input increases, the grain size of the weld increases, the corrosion current density of the weld increases, and the R_{ct} value of the weld zone gradually decreases. Consequently, increasing the wire feeding speed led to a decrease in the corrosion resistance.

Combined with the results of the tensile tests and corrosion experiments, for ensuring the weld quality, the best wire feeding speed is 8.5 mm/s, at which the weld joint has the highest corrosion resistance and the best mechanical properties.

ACKNOWLEDGEMENTS

This work was supported by the Open Project of State Key Laboratory of Comprehensive Utilization of Industrial Emission Gas under Grant SKLIVGR-SWPU-2020-04.

References

1. S. K. Sharma, S. Maheshwari, *J. Nat. Gas Sci. Eng.*, 38 (2017) 203.
2. J. A. Lee, D. H. Lee, M. Y. Seok, U. B. Baek, and Y. H. Lee, *Mater. Charact.*, 82 (2013) 17.
3. H. Zhao, B. P. Wynne, E. J. Palmiere, *Mater. Charact.*, 123 (2017) 128.
4. M. Rakhshkhorshid, H. M. Zadeh, S. H. Hashemi, *Int. J. Adv. Manuf. Technol.*, 79 (2015) 1623.
5. A. G. Kostryzhev, O. O. Marenych, C. R. Killmore and E. V. Pereloma, *Metall. Mater. Trans. A*, 46 (2015) 3470.
6. X. Chen, G. Qiao, X. Han and X. Wang, *Mater. Des.*, 53 (2014) 888.
7. A. Y. Ivanov, R. V. Sulyagin, V. V. Orlov and A. A. Kruglova, *Met. Sci. Heat Treat.*, 53 (2012) 560.
8. M. Yang, J. Lu, J. Chen, Y. Li, Y. Liu and H. Yang, *Mater. Corros.*, 71 (2019) 300.
9. P. L. Moore, D. S. Howse, E. R. Wallach, *Sci. Technol. Weld. Joining*, 9 (2004) 314.
10. S. Gook, A. Gumenyuk, M. Rethmeier, *Sci. Technol. Weld. Joining*, 19 (2014) 15.
11. O. Seffer, R. Lahdo, A. Springer and S. Kaierle, *J. Laser Appl.*, 26 (2014), 042005.

12. Y. Tian, H. T Wang, Z. D Wang, R. D. K Misra, and G. D. Wang, *J. Mater. Eng. Perform.*, 27 (2018) 1494.
13. M. Yang, Y. Liu, J. Zhang, D. Xiang, Z. Zhou and D. Wang, *Trans. Indian Inst. Met.*, 71 (2018) 2487.
14. W. Zhao, W. Wang, S. Chen and J. Qu, *Mater. Sci. Eng. A*, 528 (2011) 7417.
15. B. Guo, L. Fan, Q. Wang and Z. Fu, *Metals*, 6 (2016) 256.
16. X. N. Wang, S. H. Zhang, J. Zhou, *Opt. Lasers Eng.*, 91 (2017) 86.
17. G. Turichin, M. Kuznetsov, *Phy. Procedia*, 78 (2015) 35.
18. B. Wang, X. Liu, G. Wang, *Metall. Mater. Trans. A*, 49 (2018) 2124.
19. A. P. Teixeira, C. G. Soares, T. A. Netto and S. F. Estefen, *Int. J. Pressure Vessels Pip.*, 85 (2008) 228.
20. L. Wang, Z. Gao, Y. Liu, X. Lu, C. Wang and W. Hu, *Int. J. Electrochem. Sci.*, 14 (2019) 161.
21. X. Wang, X. Song, Y. Chen and Z. Wang, *Int. J. Electrochem. Sci.*, 13 (2018) 5654
22. T. M. Majid, S. A. R. Sultan, S. D. Mahdi and S. Jasim, *Corrosion*, 46 (1990) 37.
23. H. H. Huang, W. T. Tsai, J. T. Lee, *Corros. Sci.*, 36 (1994) 1027.
24. V. S. Voruganti, H. B. Luft, D. DeGeer and S. A. Bradford, *Corrosion*, 47 (1991) 343.
25. G. Khalaj, M. J. Khalaj, *Int. J. Pressure Vessels Pip.*, 145 (2016) 1.
26. L. W. Wang, Z. Y. Liu, Z. Y. Cui, C. W. Du, X. H. Wang and X. G. Li, *Corros. Sci.*, 85 (2014) 401.
27. K. D. Ralston, N. Birbilis, C. H. J. Davies, *Scr. Mater.*, 63 (2010) 1201.
28. L. G. Ecco, S. Rossi, F. J. Deflorian and M. Fedel, *J. Electrochem. Soc.*, 165 (2018) C933.

© 2020 The Authors. Published by ESG (www.electrochemsci.org). This article is an open access article distributed under the terms and conditions of the Creative Commons Attribution license (<http://creativecommons.org/licenses/by/4.0/>).